AMERICAN SOCIETY FOR MICROBIOLOGY | Journal of Bacteriology®

RESEARCH ARTICLE

Characterization of the *Sinorhizobium meliloti* HslUV and ClpXP Protease Systems in Free-Living and Symbiotic States

Aaron J. Ogden,[a,b] Jacqueline M. McAleer,[b] Michael L. Kahn[a,b]

[a]Molecular Plant Science Program, Washington State University, Pullman, Washington, USA
[b]Institute of Biological Chemistry, Washington State University, Pullman, Washington, USA

ABSTRACT Symbiotic nitrogen fixation (SNF) in the interaction between the soil bacteria *Sinorhizobium meliloti* and legume plant *Medicago sativa* is carried out in specialized root organs called nodules. During nodule development, each symbiont must drastically alter their proteins, transcripts, and metabolites in order to support nitrogen fixation. Moreover, bacteria within the nodules are under stress, including challenges by plant antimicrobial peptides, low pH, limited oxygen availability, and strongly reducing conditions, all of which challenge proteome integrity. *S. meliloti* stress adaptation, proteome remodeling, and quality control are controlled in part by the large oligomeric protease complexes HslUV and ClpXP1. To improve understanding of the roles of *S. meliloti* HslUV and ClpXP1 under free-living conditions and in symbiosis with *M. sativa*, we generated Δ*hslU*, Δ*hslV*, Δ*hslUV*, and Δ*clpP1* knockout mutants. The shoot dry weight of *M. sativa* plants inoculated with each deletion mutant was significantly reduced, suggesting a role in symbiosis. Further, slower free-living growth of the Δ*hslUV* and Δ*clpP1* mutants suggests that HslUV and ClpP1 were involved in adapting to heat stress, the while Δ*hslU* and Δ*clpP1* mutants were sensitive to kanamycin. All deletion mutants produced less exopolysaccharide and succinoglycan, as shown by replicate spot plating and calcofluor binding. We also generated endogenous C-terminal enhanced green fluorescent protein (eGFP) fusions to HslU, HslV, ClpX, and ClpP1 in *S. meliloti*. Using anti-eGFP antibodies, native coimmunoprecipitation experiments with proteins from free-living and nodule tissues were performed and analyzed by mass spectrometry. The results suggest that HslUV and ClpXP were closely associated with ribosomal and proteome quality control proteins, and they identified several novel putative protein-protein interactions.

IMPORTANCE Symbiotic nitrogen fixation (SNF) is the primary means by which biologically available nitrogen enters the biosphere, and it is therefore a critical component of the global nitrogen cycle and modern agriculture. SNF is the result of highly coordinated interactions between legume plants and soil bacteria collectively referred to as rhizobia, e.g., *Medicago sativa* and *S. meliloti*, respectively. Accomplishing SNF requires significant proteome changes in both organisms to create a microaerobic environment suitable for high-level bacterial nitrogenase activity. The bacterial protease systems HslUV and ClpXP are important in proteome quality control, in metabolic remodeling, and in adapting to stress. This work shows that *S. meliloti* HslUV and ClpXP are involved in SNF, in exopolysaccharide production, and in free-living stress adaptation.

KEYWORDS *Medicago sativa*, *Sinorhizobium meliloti*, ClpP, ClpX, HslU, HslV, protease, protein-protein interaction, symbiosis, symbiotic nitrogen fixation

Symbiotic nitrogen fixation (SNF) is the process whereby inert atmospheric dinitrogen is reduced to ammonium by specialized prokaryotes living in partnership with a eukaryotic host. In terrestrial systems, symbiotic interactions between alpha- and

Citation Ogden AJ, McAleer JM, Kahn ML. 2019. Characterization of the *Sinorhizobium meliloti* HslUV and ClpXP protease systems in free-living and symbiotic states. J Bacteriol 201:e00498-18. https://doi.org/10.1128/JB.00498-18.

Editor Anke Becker, Philipps-Universität Marburg

Address correspondence to Michael L. Kahn, kahn@wsu.edu.

Received 17 October 2018
Accepted 15 January 2019
Accepted manuscript posted online 22 January 2019
Published 13 March 2019

betaproteobacteria and various legumes result in the largest input of biologically available nitrogen into the biosphere, making these interactions a critical component of global nitrogen cycling and modern agriculture.

An agriculturally relevant example of SNF occurs between the Gram-negative alphaproteobacterium *Sinorhizobium meliloti* and the pasture legume *Medicago sativa* (alfalfa). This relationship has been studied as a model for SNF. The highly developed symbiosis between these two organisms begins when the roots of nitrogen-deprived alfalfa excrete a characteristic set of flavonoids into the surrounding rhizosphere. The rhizobia are stimulated by these flavonoids to produce specific lipochitooligosaccharides, which alter alfalfa root growth, morphology, and cell division. The chemical dialogue results in the intracellular uptake of rhizobia into the root and the *de novo* generation of a novel organ, the root nodule.

Within root nodules, *S. meliloti* and alfalfa reorganize their metabolism to establish the conditions necessary for nitrogen fixation. We now understand that this metabolic remodeling involves subjecting rhizobia to seemingly hostile cellular conditions, including microaerobicity (1), challenge by plant-derived antimicrobial peptides (2) and plant proteases (3), decreased pH (4), osmotic stress (5), and oxidative bursts (6). These and other conditions result in terminally differentiated nitrogen-fixing forms of the rhizobia called bacteroids. Relative to free-living bacteria, bacteroids are larger, are often branched, and have undergone multiple rounds of endoreduplication. Nitrogen-fixing bacteroids have been shown to have a drastically altered transcriptome (7, 8) and proteome (9) compared to those of their non-nitrogen-fixing counterparts.

The unique metabolic conditions necessary for successful nitrogen fixation have been studied extensively at the transcript level, but little is known about the role of protein quality control and turnover in SNF. The rhizobial protein complexes HslUV (SMc02577 and SMc02575, respectively) and ClpXP1 (SMc01904 and SMc01903, respectively) form large oligomeric barrel-shaped structures composed of an unfoldase (HslU and ClpX) and a protease (HslV and ClpP1). In both systems the unfoldase uses ATP hydrolysis to linearize folded proteins and translocate these into the protease for proteolysis (10). Bacterial HslUV and ClpXP1 complexes are orthologous to eukaryotic 26S proteasomes and function similarly to maintain the integrity of the cell's proteome by degrading damaged or misfolded protein. Furthermore, work in multiple bacterial systems has shown that both protease systems carry out targeted degradation of regulatory proteins and are involved in many cellular processes, including the SOS response (11), cell cycle regulation (12), heat stress (13, 14), polysaccharide biosynthesis (15), pilus formation and DNA transfer (16), RNA metabolism (17), and SNF (12). Furthermore, exposing *S. meliloti* to conditions found within root nodules, including incubation with legume host-derived antimicrobial peptide NCR335 (2) or shifting growth media to acidic pH (18), results in increased expression of *clpXP1* and *hslUV*. Interestingly, *clpX* has been established as one of the minimal suite of genes necessary for nitrogen fixation in the nonnodulating diazotroph *Azotobacter* (19) and is necessary for cell growth in *S. meliloti* (12). *S. meliloti* contains other similar protease systems, including *ftsH* (SMc04459) and *lon* (SMc01905), and the unfoldase *clpA* (SMc02109). Unlike the case for *clpX*, *hslU*, and *hslV*, the *S. meliloti* genome contains two additional *clpP* genes, *clpP2* (SMc02720) and *clpP3* (SMc03841). While *clpXP1* and *hslUV* occur as chromosomal operons, these *clpP* genes are located far from their cognate partner *clpX*. Further, the SMc02720 and SMc03841 protein sequences show only 37% and 60% identity with the canonical *Escherichia coli* ClpP, respectively, compared to a 72% protein sequence identity of ClpP1.

While HslUV and ClpXP are known to play critical roles in prokaryotic protein homeostasis and targeted protein degradation, little is known about their function in SNF. In this study, we evaluated the transcriptional response of *S. meliloti hslUV* and *clpXP1* to various abiotic stresses and characterized the phenotypes of Δ*hslU*, Δ*hslV*, Δ*hslUV*, and Δ*clpP1* deletion mutants under free-living conditions and in symbiosis with *M. sativa*. We were able to localize HslUV and ClpXP1 proteins within the nodule by confocal microscopy of protein-green fluorescent protein (GFP) fusions. Finally, we

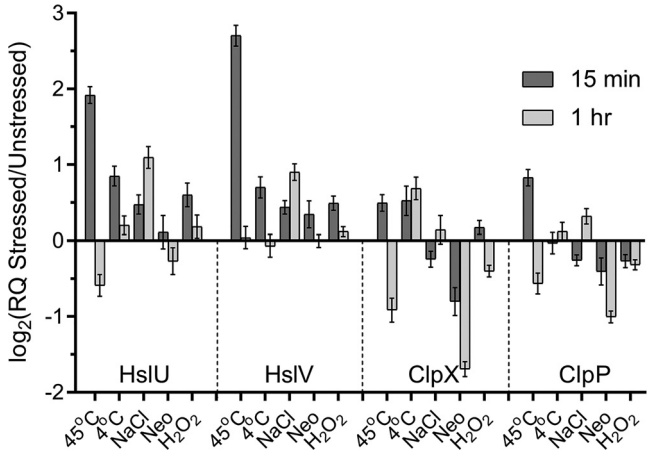

FIG 1 Transcriptional stress response of *hslUV* and *clpXP1*. The transcriptional response of *hslUV* and *clpXP* was investigated by comparing RQ ($2^{-\Delta\Delta CT}$) values of stressed and unstressed cultures, in biological triplicate, at 15 min and 1 h poststress. Error bars indicate the average RQ maximum and minimum values for the biological triplicates. Neo, neomycin.

present a list of proteins that coimmunoprecipitated with these GFP fusion proteins in free-living and symbiotic cells and suggest ways that these may interact with the HslUV and ClpXP proteasome systems.

RESULTS

HslUV and ClpXP respond transcriptionally to multiple stresses. Transcriptional start site and promoter analysis suggested the *hslUV* and *clpXP1* operons are under the control of the RpoD, RpoH1, and RpoH2 transcription factors (20). To gain a more comprehensive understanding of the transcriptional control of these genes, we subjected wild-type *S. meliloti* to various stresses for 15 or 60 min and then isolated bacterial RNA and used quantitative PCR (qPCR) to evaluate changes that had occurred at these times (Fig. 1). As previously observed, both *hslU* and *hslV* were induced at 15 min after heat shock (21). The *hslU* and *hslV* genes were also induced by cold shock, elevated salt stress, and, to a lesser extent, oxidative stress. The *clpX* and *clpP1* genes were moderately induced in response to heat shock but did not appear to be positively or negatively regulated by elevated salt stress or H_2O_2 treatment. Interestingly, neomycin stress appeared to lower *clpXP1* expression. In most cases, transcript abundances apparently returned to unstressed levels after 1 hour or were reduced to below unstressed transcript levels. This suggests that during chronic heat and neomycin stresses, either the *clpXP1* genes are negatively regulated or their transcripts are less stable than the reference transcript.

HslUV and ClpP1 contribute to normal growth, EPS production, and symbiosis. To test the impact of functional HslUV and ClpXP1 systems in *S. meliloti*, we generated Δ*hslU*, Δ*hslV*, Δ*hslUV*, and Δ*clpP1* deletion mutants. It had been previously shown that inactivating *clpX* is lethal to *S. meliloti* (12), which we also observed (data not shown). Figure 2 shows the effects of various deletion mutations on doubling times of free-living cells growing in nutrient-rich LB medium. Under normal laboratory growth conditions, all deletion strains exhibited only minor growth defects. Despite the continued activity of the homologous *clpP2* gene, growth of the Δ*clpP1* mutant was most impaired. Under elevated temperatures simulating a chronic heat stress, the growth of each deletion mutant was inferior, with Δ*hslU*, Δ*hslV*, Δ*hslVU*, and Δ*clpP1* strains reaching final A_{600}s of 0.12, 0.15, 0.21, and 0.08, respectively, compared to an A_{600} of 0.28 for wild-type Rm1021 (Fig. 2, middle panel). Similarly, addition of a sublethal concentration of kanamycin caused poor growth of the deletion mutants, resulting in final A_{600}s for the Δ*hslU*, Δ*hslVU*, and Δ*clpP1* strains of 0.16, 0.19, and 0.09, respectively, compared to 0.27 for Rm1021. Interestingly, kanamycin did not impact the growth of

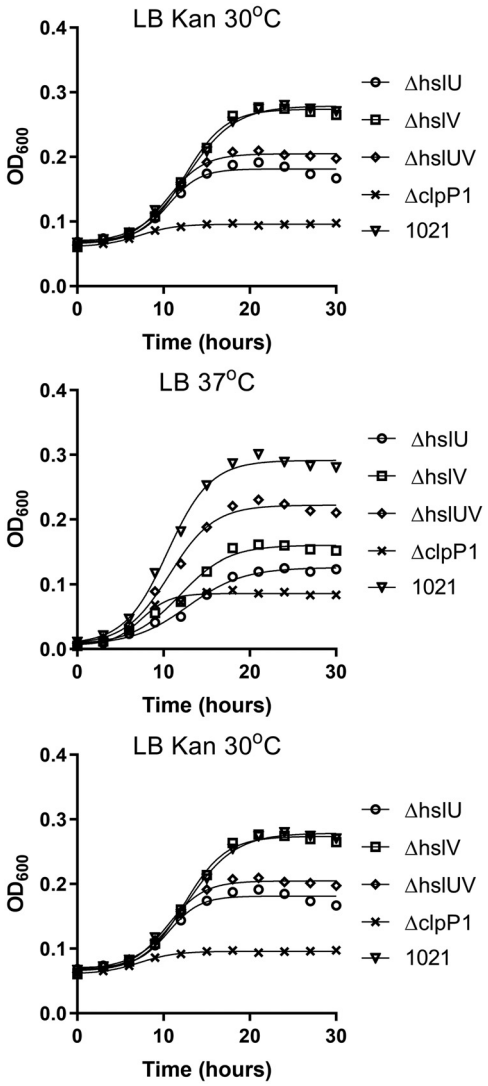

FIG 2 Growth curve phenotypes of protease and unfoldase mutants in liquid culture. Wild-type Rm1021 and deletion mutants were grown under optimal conditions (top), with chronic elevated heat (middle), or at optimal temperature supplemented with kanamycin (bottom). While growth under optimal conditions appears to have a mild impact on the final A_{600}, the growth of each mutant is impaired by a chronic heat stress and kanamycin stress (except for the Δ*hslV* mutant under kanamycin stress [bottom]).

the Rm1021 Δ*hslV* mutant, which reached a final A_{600} comparable to that of the wild type (Fig. 2, bottom panel). Furthermore, under heat stress, the Δ*hslVU* double deletion mutant reached a final A_{600} higher than that of either the Δ*hslU* or Δ*hslV* mutant.

Unfoldase and protease deletions also resulted in lower production of exopolysaccharides (EPS) (Fig. 3). Synchronized cultures normalized to the same optical density were spotted onto nutrient-rich and minimal media. On both media, the deletion mutants appeared to produce significantly less exopolysaccharide. Succinoglycan (EPSI) is a symbiotically important exopolysaccharide (22) that binds calcofluor, a fluorescent whitener dye, and the interaction can be visualized by fluorescence under UV light. Compared to that in the wild-type Rm1021, the level of succinoglycan-related fluorescence was lower in the Δ*hslU*, Δ*hslV*, Δ*hslUV*, and Δ*clpP1* mutant strains on LB medium and, to a lesser extent, on minimal medium supplemented with mannitol ($MMNH_4$) (Fig. 3, bottom panels).

To test the impact of these mutations on symbiosis, each deletion mutant was used to inoculate *M. sativa* seedlings, and plants were grown for 28 days under optimal and

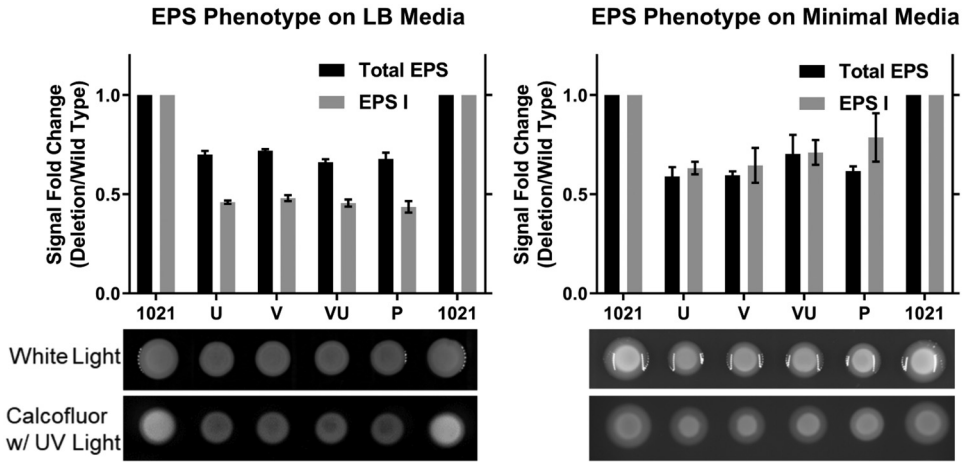

FIG 3 Exopolysaccharide and succinoglycan are reduced in deletion strains. The production of total polysaccharide (top row of plates) and succinoglycan (bottom row of plates) were visualized on both LB (left) and $MMNH_4$ (right) media for both wild-type Rm1021 and deletion strains. Supplementing the growth media with calcofluor white allowed succinoglycan visualization under UV light. The brightness of each colony was measured using the Fiji image analysis package and is represented as a fold change compared to the wild-type Rm1021 (bar graphs).

elevated temperatures. Figure 4 shows that the *S. meliloti* Δ*hslU*, Δ*hslV*, and Δ*hslUV* mutants led to significant 22%, 21%, and 15% reductions in plant dry weight, respectively (two-tailed *t* test, $P < 0.001$). The Δ*clpP1* mutant had a larger effect, with a significant 30% reduction in plant dry weight. The same phenotypic trend was observed under heat stress conditions (Fig. 4, middle). As expected, the addition of a chronic heat stress caused the shoot dry weights of plants inoculated with the Δ*hslU*, Δ*hslV*, Δ*hslVU*, and Δ*clpP1* deletion strains to decrease further, resulting in significant 29%, 29%, 17%, and 36% reductions, respectively.

HslUV and ClpXP protein distributions are not zone specific. Nodules formed in the symbiosis between *M. sativa* and *S. meliloti* are indeterminate and form developmental zones along the nodule longitudinal axis, each containing unique protein, metabolite, and transcript profiles (8, 9). Therefore, if HslUV and ClpXP proteins accumulate in particular zones within the nodule, this may indicate that they play a specific role in SNF development or that their protein-protein interactions would be limited to gene products in that region. To determine the locations of HslUV and ClpXP proteins, we generated C-terminal enhanced GFP (eGFP) fusions to these proteins and homologously recombined the genes coding for these fusions into the genome in order to

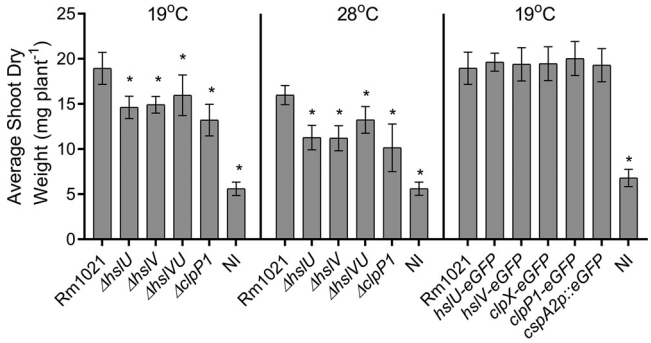

FIG 4 Effect of deletions and eGFP fusions on shoot dry weight. Deleting *hslU*, *hslV*, *hslVU*, and *clpP1* led to a significant decrease in shoot dry weight compared to that with wild-type *S. meliloti* Rm1021 (two-tailed *t* test, $P < 0.05$ [asterisks]). A similar but slightly greater inhibition was observed at elevated temperatures. Fusing eGFP to the C terminus of HslU, HslV, ClpX, or ClpP1 or expression of eGFP from the *cspA2* promoter had no significant effect on plant dry weight (two-tailed *t* test, $P > 0.05$). NI, noninoculated.

make their expression depend on their endogenous promoters. These fusions did not appear to affect symbiotic productivity, as shown in Fig. 4 (right), and no obvious free-living growth phenotype was observed in solid or liquid media (data not shown). Using confocal microscopy of *M. sativa* nodules, we located *S. meliloti* HslU-eGFP, HslV-eGFP, ClpX-eGFP, and ClpP1-eGFP during symbiosis. Figure 5 shows that neither HslUV, ClpXP, nor eGFP driven by the *cspA2* promoter appeared to be located in particular zones. Further, each protein occasionally appeared to be concentrated in small, punctate domains (Fig. 5, arrows), a finding previously described for another ClpXP system (12) and not observed in our *cspA2p*::*eGFP* samples.

HslUV and ClpXP interact with translation and protein folding machinery in free-living and symbiotic life stages. To gain a better understanding of HslUV and ClpXP function in rhizobia, we conducted native coimmunoprecipitation (co-IP) experiments using HslU-eGFP, HslV-eGFP, ClpX-eGFP, and ClpP1-eGFP fusion constructs. Using mass spectrometry (MS), we then determined which proteins were associated with eGFP in free-living *S. meliloti* and in alfalfa nodules. As a control to determine which proteins identified by co-IP and MS might be interacting directly with the C-terminal eGFP tag, we constructed an *S. meliloti* strain in which an eGFP protein without an N-terminal fusion was expressed under the control of the *cspA2* (SMc01428) promoter in a similar construct. Recombining sequences into the genome eliminated issues with maintaining a plasmid for heterologous expression during symbiosis and also provided ordinary control of copy number.

To identify weaker interactions that may occur on the exterior of the complex, as well as stronger interactions that may occur within the complex, coimmunoprecipitations with HslU-eGFP, HslV-eGFP, ClpX-eGFP, ClpP1-eGFP, and P_{cspA2}-eGFP were performed by using both a low-volume wash (2×10 column volumes) and a higher-volume wash (2×100 column volumes). The effectiveness of the co-IP was monitored by Western blot analysis using anti-eGFP antibodies (Fig. 6). Proteins that coprecipitated with eGFP-tagged proteasome proteins were identified via MS (see Tables S2 and S3 in the supplemental material), and their abundances were compared to those of proteins isolated from the eGFP protein coprecipitation. Proteins were considered identified when they were represented by two or more unique peptides and were considered to be enriched when they were at least twice as abundant in the co-IP with a specific protein-eGFP fusion than they were in the control co-IP with P_{cspA2}-eGFP.

To validate the success of our co-IPs, we compared the proteins observed to coprecipitate with our eGFP-tagged proteins with previously experimentally validated interactors in *Mesorhizobium loti* (23). Because few studies of global protein-protein interactions have been done in rhizobia, we also included proteasome interactions identified in *Escherichia coli* (24–28). We also chose to compare our coprecipitated proteins with those proteins that were confidently predicted (high confidence score of >0.7) to interact with HslUV and ClpXP1 in the STRING database using *Sinorhizobium meliloti* Rm1021 and *Escherichia coli* K-12 (29). The STRING database is a powerful tool that uses text mining, coexpression, cooccurrence, and other analyses with data compiled from a large number of organisms. A compilation of HslUV and ClpXP1 protein-protein interactions experimentally identified or confidently predicted by STRING, as well as experimentally identified interactors in *E. coli* and *Mesorhizobium*, is available in Table S4 in the supplemental material. As summarized in Fig. 7, our free-living co-IPs identified many proteins that had previously been found to interact with HslUV and ClpXP1. While many known interactors were identified in nodule co-IPs, fewer of these proteins were >2-fold enriched compared to the background. Because the HslUV and ClpXP1 systems function as oligomeric complexes, we compared the proteins that were >2-fold enriched by association with the unfoldases, HslU-eGFP and ClpX-eGFP, with results obtained using their partner proteases, HslV-eGFP and ClpP1-eGFP, respectively. Figure 8 illustrates that under free-living conditions, 48% of the proteins enriched in the HslU-eGFP co-IP were also enriched in the HslV co-IP, and 72% of the proteins enriched in the ClpX-eGFP co-IP were enriched in the ClpP1-eGFP co-IP.

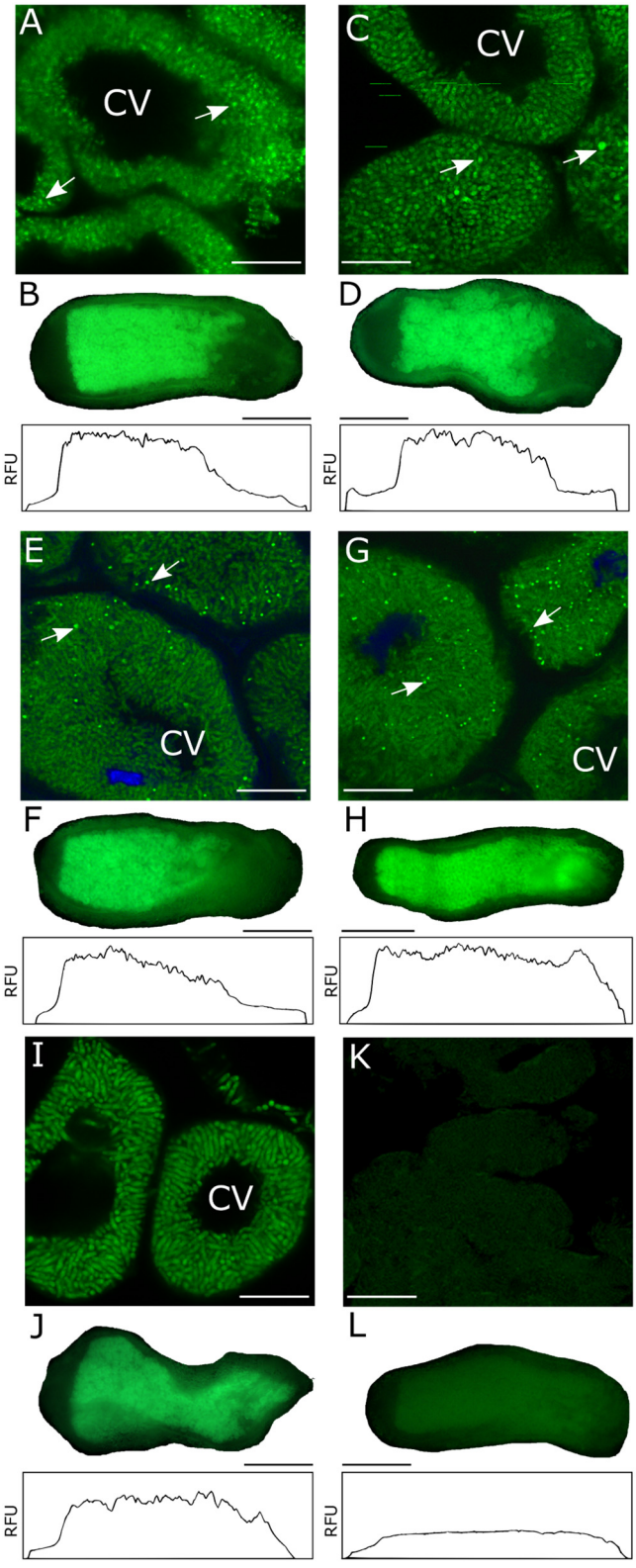

FIG 5 Unfoldase- and protease-eGFP localization within the nodule. eGFP fluorescence was visualized at a magnification of ×250 (A, C, E, G, I, and K) (scale bars = 10 μm) or ×10 (B, D, F, H, J, and L) (scale bars = 1 mm) for nodules inoculated with Rm1021 *hslU-eGFP* (A and B), *hslV-eGFP* (C and D), *clpX-eGFP* (E and F), *clpP1-eGFP* (G and H), or *cspA2p*::*eGFP* (I and J) or wild-type Rm1021 (K and L). The appearance of punctate foci is marked with arrows. Fiji image analysis software tracks the total fluorescence across the longitudinal axis of the nodules below each ×10 image. CV, central vacuole.

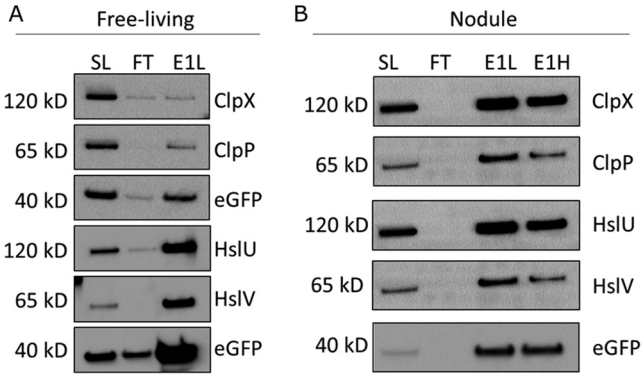

FIG 6 Western blot analysis of coimmunoprecipitation experiments. Each unfoldase- and protease-eGFP fusion, as well as eGFP expressed from the P_{cspA2} promoter, was purified from spun lysates of free-living *S. meliloti* (A) and alfalfa nodules (B) using camelid anti-eGFP agarose-conjugated antibodies. The efficiency of the process was visualized using a Western blot probed with rabbit anti-eGFP. SL, spun lysate; FT, flowthrough; E1L, elution low wash; E1H, elution high wash.

The overlap in similarly enriched proteins decreased in nodule experiments to 21% and 36% for HslUV and ClpXP1, respectively.

To understand whether HslUV and ClpXP1 preferentially targeted gene products produced from the different megaplasmids, we conducted hypergeometric tests and determined Bonferroni-adjusted *P* values. As summarized in Fig. S1 in the supplemental material, proteins located on the chromosome were significantly overrepresented in both HslUV and ClpXP1 co-IPs, with the exception of the HslV-eGFP nodule sample. Proteins from pSymA and pSymB were significantly underrepresented under free-living conditions but had no significant over- or underrepresentation in nodule co-IPs.

We also used gene ontology (GO) enrichment analysis to determine whether the proteins that coprecipitated with HslUV or ClpXP1 were associated with specific biological processes (30). We found that under free-living conditions, HslU-eGFP, ClpX-eGFP, and ClpP1-eGFP were enriched 2.6-, 6.7-, and 6.2-fold, respectively, for proteins associated with translation (Fig. 9). In addition, ClpX- and ClpP1-eGFP were enriched 7.3- and 6.9-fold, respectively, for members of the protein-folding biological process. Similarly, during symbiosis, HslU-eGFP, HslV-eGFP, and ClpX-eGFP were enriched for *S. meliloti* translation-associated proteins by 6.9-, 5.5-, and 9-fold, respectively. HslU-eGFP was also 8.8-fold enriched for bacterial glycolysis-associated proteins. The *S. meliloti* HslV-eGFP nodule co-IP showed enrichment for a number of host plant *M. sativa* proteins with biological processes including the tricarboxylic acid (TCA) cycle, glycolysis, and H_2O_2 catabolism, as well as translation initiation and preinitiation complexes.

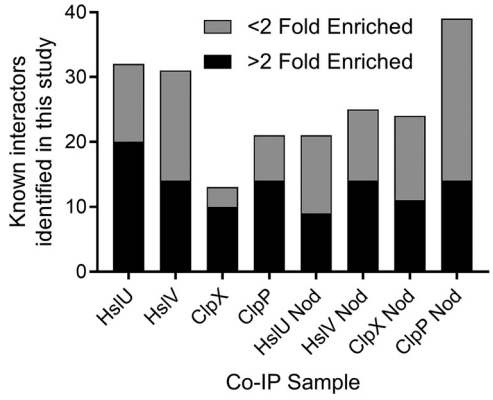

FIG 7 Enrichment analysis of known interactors. As described in the text, many proteins that are known or predicted to interact with HslUV and ClpXP1 were identified in this study. Under free-living conditions, most of those proteins are enriched above the background sample by ≥2-fold.

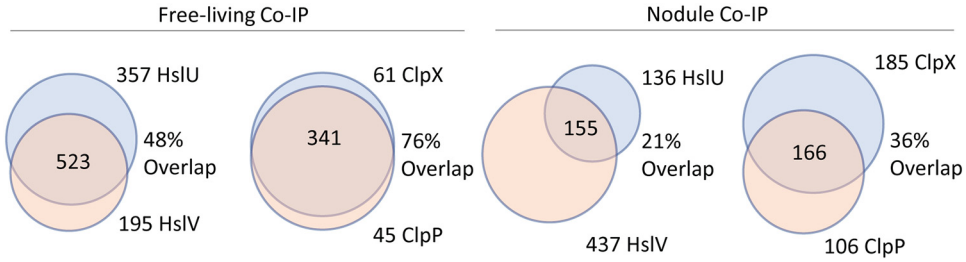

FIG 8 Venn diagram showing overlap of ≥2-fold-enriched proteins in HslUV-eGFP and ClpXP1-eGFP coimmunoprecipitations. Numbers outside the circles represent the number of proteins found exclusively enriched in that sample. Numbers in the overlap represent the shared proteins.

Because our co-IPs used lysed nodule tissue and not isolated symbiosomes, it remains a possibility that *M. sativa* plant proteins observed to interact with HslUV or ClpXP1 occurred only after nodule lysis. As a result, we have not evaluated the hypothesis that these proteins are secreted into the symbiosome. However, all plant proteins identified in this study were evaluated for the presence of an N-terminal secretion signal via the SignalP (v4.1, default d-cutoff value), and these results are summarized in Table S3 (31).

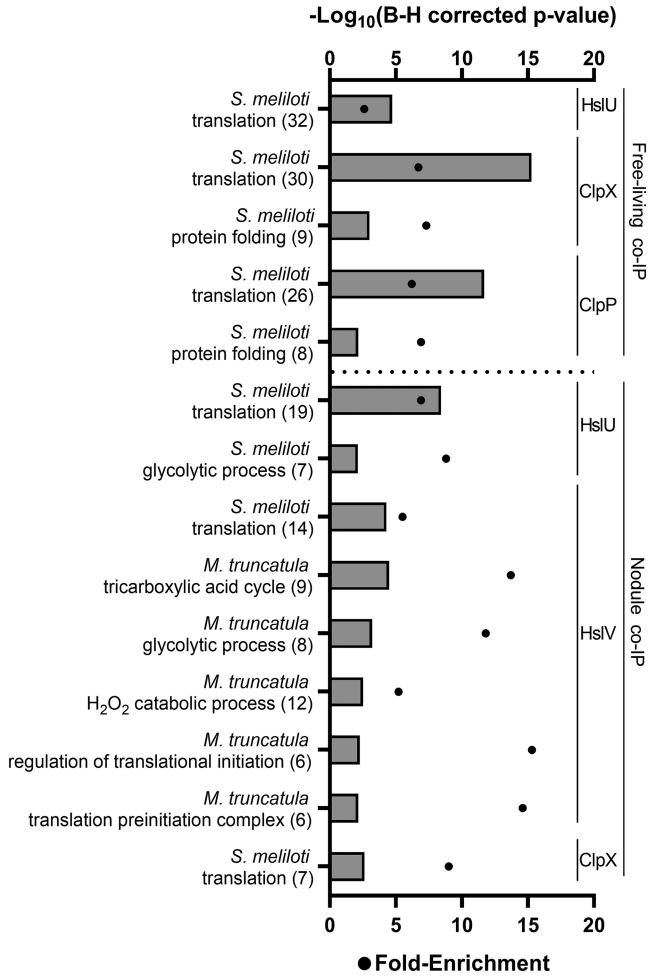

FIG 9 Gene ontology enrichment of coimmunoprecipitated proteins. Gene Ontology Consortium terms were used in an enrichment analysis of proteins that coimmunoprecipitated with eGFP-tagged HslU, HslV, ClpX, or ClpP1 at least ≥2-fold compared to the eGFP control. The number of proteins contributing to each ontological class is shown in parentheses for each row.

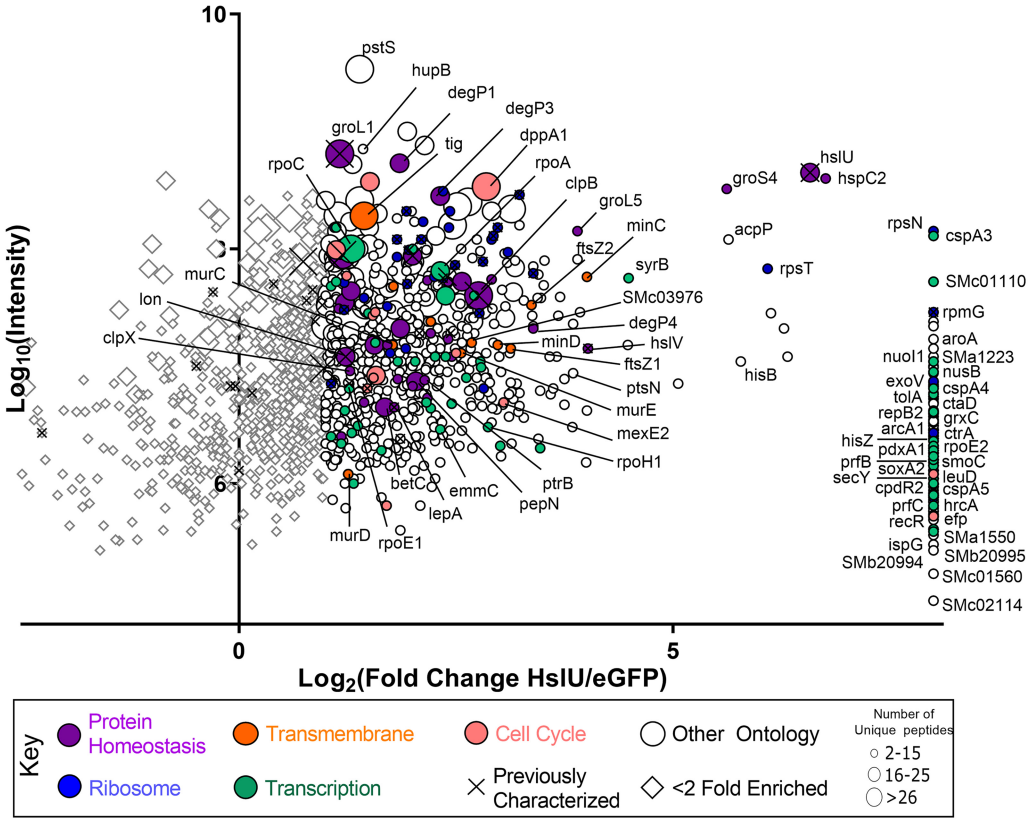

FIG 10 Log-log bubble graph showing proteins enriched in HslU-eGFP coimmunoprecipitations. The intensities of proteins that coprecipitate with *S. meliloti* HslU-eGFP target and *cspA2p*::eGFP background samples under free-living conditions were expressed as a $\log_2$ fold change (target/background) along the *x* axis. Protein intensities were $\log_{10}$ transformed and plotted along the *y* axis. Fold change values could not be calculated for proteins found in the target co-IPs but not in the eGFP immunoprecipitation (i.e., target protein intensity/background protein intensity = *x*/0), so they were all assigned the same arbitrary value at the far right of the *x* axis.

All proteins that coprecipitated in the different co-IPs are included in Tables S2 and S3. We have summarized these data graphically for each co-IP (Fig. 10; see Fig. S2 in the supplemental material). Figure 10, for example, displays each coprecipitated protein as a function of $\log_2$ fold enrichment on the *x* axis versus the $\log_{10}$ signal intensity on the *y* axis. Proteins with <2-fold enrichment are shown as diamonds, while >2-fold-enriched proteins are represented as circles. In all cases, only proteins with >2 unique peptides are shown. For proteins that were not detected in the background eGFP co-IP but were confidently identified in the unfoldase or protease co-IPs (i.e., sample signal/background signal = 0), an arbitrary $\log_2$ fold change value was assigned to align each feature on the far right of the *x* axis. The size of each feature reflects the number of unique peptides that contributed to the identification of its parent protein. The color of each feature represents a different protein ontology, and previously characterized or predicted protein-protein interactions are overlaid as an "x" symbol.

DISCUSSION

Symbiotic nitrogen fixation between rhizobia and legumes is a critical component of global nitrogen cycling and agriculture. To accomplish SNF, both organisms must coordinate and maintain a drastic metabolic shift from free-living individuals to a symbiotic pair. While this shift has been studied extensively at the transcript level, little is known about the role of protein quality control and turnover in symbiosis. Here, we further characterized the roles of two *S. meliloti* operons that code for proteasomes, *hslUV* (SMc02577 and SMc02575) and *clpXP1* (SMc01904 and SMc01903), in free-living cells and in symbiosis with *M. sativa*. We confirmed that under free-living conditions

both *hslUV* and *clpXP1* respond transcriptionally to heat stress (20). We then showed that *hslUV* transcription was induced by low temperature and high NaCl stress and to lesser extent by treatment with H_2O_2. A recent mRNA microarray experiment following H_2O_2 treatment showed signal log ratios of 2.1 and 1.8 for *hslU* and *hslV*, respectively, which is in rough agreement with our findings (32). Furthermore, we showed that *clpXP1* expression was repressed by treatment with low concentrations of the aminoglycoside antibiotic neomycin, which was expected to increase the frequency of amino acid misincorporation and thereby alter protein stability (33). Although we anticipated induction of *hslUV* and *clpXP1* in response to treatment with neomycin, it has been shown that different aminoglycosides can have drastically different impacts on expression of protein homeostasis genes in *Bacillus subtilis* (34).

To evaluate whether *S. meliloti hslUV* or *clpP1* gene products were necessary for free-living growth and efficient symbiosis with *M. sativa*, we generated Δ*hslU*, Δ*hslV*, Δ*hslUV*, and Δ*clpP1* knockout mutants. These had a minor decrease in free-living doubling times without stress, but there was a much more drastic effect on growth rate and yield when the mutants were subjected to heat or neomycin treatment. Interestingly, the effect on growth at 30°C and 42°C after deleting both *hslU* and *hslV* (Δ*hslUV*) was less severe than that of deleting each gene alone, suggesting aberrant activity by the remaining subunit when it was not properly coupled to the missing component. Similarly, growth of the Δ*hslU*, Δ*hslUV*, and Δ*clpP1* mutants was severely inhibited in response to kanamycin treatment, while the Δ*hslV* mutant grew at wild-type rates, suggesting that Δ*hslV* was not involved in dealing with the consequences of kanamycin treatment. Furthermore, each mutant exhibited a visible reduction in total EPS and EPSI production. All mutation constructs had a statistically significant negative effect on symbiosis with *M. sativa*. As with free-living growth curve experiments, the phenotype of the Δ*hslUV* double deletion mutant was less severe than those of the individual Δ*hslU*, Δ*hslV*, and Δ*hslUV* mutants. The symbiotic phenotype of these mutants may be caused by decreased EPS or EPSI production, although we observed no difference in total nodule numbers or color (data not shown). These findings strongly suggest that *hslUV* and *clpP1* play important roles in SNF.

Constructs containing *S. meliloti* HslU, HslV, ClpX, and ClpP1 proteins that had been C-terminally tagged with eGFP were expressed from their native promoters and were used to locate these proteins within root nodules. There appeared to be no zone specificity of expression. ClpX-eGFP and ClpP1-eGFP formed punctate foci, as previously described (12). Interestingly, HslU- and HslV-eGFP also appeared to form punctate loci, although to a lesser extent than ClpXP1-eGFP. The lack of zone specificity for HslUV-eGFP and ClpXP1-eGFP was consistent with previous studies (8, 9).

To identify proteins that interacted with the proteasomes, we conducted a native co-IP experiment using eGFP-tagged HslUV and ClpXP1 proteins present in *S. meliloti* under free-living conditions and in symbiosis with *M. sativa*. As a control to identify proteins carried into the proteomic analysis by interacting with the beads, tubes, or eGFP, we also used an *S. meliloti* strain expressing eGFP from the *cspA2* promoter (*cspA2p::eGFP*). Our data supported many experimentally validated and computationally predicted HslUV and ClpXP1 protein-protein interactions. Consistent with their function as an oligomeric complex, we showed strong similarity in the proteins enriched in the HslU-eGFP and HslV-eGFP co-IPs, as well as in the ClpX-eGFP and ClpP1-eGFP samples. During symbiosis, however, the profile of HslU-eGFP and ClpX-eGFP coeluting proteins was much different from that under free-living conditions, suggesting additional roles outside their established partnerships. This observation, however, may be influenced by large amounts of plant proteins brought into close proximity with HslUV and ClpXP1 due to lysing of nodule tissue. Hypergeometric statistical tests revealed that under all but one experimental condition, the HslUV and ClpXP1 coeluting proteins were significantly overenriched for proteins encoded on the chromosome. Proteins from pSymA and pSymB were significantly underrepresented in free-living co-IPs but were neither over- nor underrepresented in nodule co-IPs.

TABLE 1 Strains and plasmids used in this study

Strain or plasmid	Genotype or relevant features[a]	Reference or source
Strains		
S. meliloti		
Rm1021	Wild-type rhizobial strain	22
Rm1021 Δ*hslU*	Rm1021 lacking *hslU* gene, SMC02577	This study
Rm1021 Δ*hslV*	Rm1021 lacking *hslV* gene, SMc02575	This study
Rm1021 Δ*hslUV*	Rm1021 lacking both *hslU* and *hslV* genes	This study
Rm1021 Δ*clpP1*	Rm1021 lacking *clpP1* gene, SMc01903	This study
Rm1021 *hslU-eGFP*	Rm1021 with integrated pK19, *hslU-eGFP* Km^r	This study
Rm1021 *hslV-eGFP*	Rm1021 with integrated pK19, *hslV-eGFP* Km^r	This study
Rm1021 *clpX-eGFP*	Rm1021 with integrated pK19, *clpX-eGFP* Km^r	This study
Rm1021 *clpP1-eGFP*	Rm1021 with integrated pK19, *clpP1-eGFP* Km^r	This study
Rm1021 *cspA2p::eGFP*	Rm1021 with integrated pK19, *cspA2* promoter-*eGFP* fusion, Km^r	
E. coli S17-1	*pro hsdR recA* [RP4-2(Tc::Mu) (Km::Tn*7*)]	47
Plasmids		
pETGFP	pET eGFP LIC u-msfGFP (Addgene plasmid no. 29772), Amp^r	Scott Gradia
pETGFP_UeGFP	u-msfGFP containing Rm1021 *hslU* coding sequence, Amp^r	This study
pETGFP_VeGFP	u-msfGFP containing Rm1021 *hslV* coding sequence, Amp^r	This study
pETGFP_XeGFP	u-msfGFP containing Rm1021 *clpX* coding sequence, Amp^r	This study
pETGFP_PeGFP	u-msfGFP containing Rm1021 *clpP1* coding sequence, Amp^r	This study
pK19 *mob sacB*	pUC19 derivative, *lacZ*α *mob sacB*, Km^r	49
pK19_UDEL	0.5-kb 5′ and 3′ flanking *hslU* fragments cloned into pK19 *mob sacB*	This study
pK19_VDEL	0.5-kb 5′ and 3′ flanking *hslV* fragments cloned into pK19 *mob sacB*	This study
pK19_PDEL	0.5-kb 5′ and 3′ flanking *clpP1* fragments cloned into pK19 *mob sacB*	This study
pK19_UeGFP	*hslU-eGFP* subcloned from pETGFP_UeGFP into pK19 *mob sacB*	This study
pK19_VeGFP	*hslV-eGFP* subcloned from pETGFP_VeGFP into pK19 *mob sacB*	This study
pK19_XeGFP	*clpX-eGFP* subcloned from pETGFP_XeGFP into pK19 *mob sacB*	This study
pK19_PeGFP	*clpP1-eGFP* subcloned from pETGFP_PeGFP into pK19 *mob sacB*	This study

[a]Km^r, kanamycin resistance; Amp^r, ampicillin resistance.

HslUV and ClpXP1 associate with ribosomal protein and nascent protein quality control systems. Nascent protein folding can be compromised by environmental stresses, intrinsically unfavorable folding thermodynamics, translation of aberrant transcripts, and other factors. Poor protein folding can lead to dysfunctional proteins, aggregation, and cell death. It is therefore reasonable that the process of refolding or degrading misfolded proteins must be immediate to ensure proteome integrity. Indeed, the ribosome and its associated proteins are increasingly being recognized as a central hub for the protein quality control machinery (35). Many proteins, including trigger factor (TF) (36), DnaJ, DnaK, and GrpE (37, 38), GroEL and GroES (39, 40), and SecA and SecB (41, 42), have been shown to act cotranslationally on nascent protein exiting the ribosome.

In this study, we observed a significant enrichment for many proteins associated with the GO biological process "translation" (predominately ribosomal proteins) in free-living HslU-eGFP, ClpX-eGFP, and ClpP1-eGFP co-IPs, as well as in HslU-eGFP, HslV-eGFP, and ClpX-eGFP nodule co-IPs. We also observed significant enrichment for the GO biological process "protein folding" in free-living co-IPs of ClpX-eGFP and ClpP1-eGFP. In many cases this includes the proteins TF, DnaJ, DnaK, GrpE, GroEL, GroES, SecA, and SecB (see Tables S2 and S3 in the supplemental material). These data implicate HslUV and ClpXP1 systems in the maintenance of the proteome integrity via direct or indirect interactions with ribosomal protein complexes and other protein quality control systems.

MATERIALS AND METHODS

***Sinorhizobium meliloti* and *Medicago sativa* growth conditions.** The strains and plasmids used in the study are listed in Table 1. *S. meliloti* was grown on minimal medium supplemented with mannitol (1% wt/vol) ($MMNH_4$) or in LB (43) unless otherwise noted. Seeds were surface sterilized as described previously (9). *M. sativa* Ladak (Bruce Seed Farm, lot no. A6-008) was grown in closed Magenta boxes to eliminate the risk of contamination with alternate *S. meliloti* strains. Each Magenta box contained plant nutrient solution (PNS) (44) lacking a nitrogen source to encourage symbiosis with rhizobia. To inoculate, rhizobia were grown to log phase in minimal medium, spun down, washed twice, and resuspended in

0.85% NaCl to a final A_{600} value of 0.1, and then 1 ml of the resuspended cells was added to each box. Plants were grown in a growth chamber with 24 h of light at 20°C.

eGFP tagging of endogenous *S. meliloti* HslUV and ClpXP unfoldases and proteases. To create a C-terminal eGFP fusion of each protease and unfoldase, the *hslU* (SMc02577), *hslV* (SMc02575), *clpX* (SMc01904), and *clpP1* (SMc01903) coding sequences were cloned as amplified PCR products into the pET eGFP ligation-independent cloning (LIC) vector u-msfGFP (Addgene plasmid no. 29772) using primers listed in Table S1 in the supplemental material and the manufacturer's protocol on LB containing 50 μg/ml ampicillin (45). The pET GFP LIC cloning vector was a gift from Scott Gradia. The *hslU-eGFP*, *hslV-eGFP*, *clpX-eGFP*, and *clpP1-eGFP* sequences from the resulting plasmids were amplified from the newly constructed u-msfGFP vectors using primers listed in Table S1, digested, ligated into pK19 *mob sacB*, and selected for using LB containing 40 μg/ml kanamycin. The resulting plasmids were then purified and transformed into the *E. coli* host S17-1, which was used to mobilize each new pK19 construct into *S. meliloti* Rm1021 via biparental mating (46, 47). Selection for neomycin-resistant exconjugants was accomplished using $MMNH_4$ containing 200 μg/ml neomycin. These plasmids are unable to replicate in *S. meliloti*, so this selection recovers cells in which the plasmids have integrated into the chromosome by homologous recombination. To produce an *S. meliloti* Rm1021 strain constitutively producing eGFP from the chromosome, we amplified the eGFP-coding sequence from u-msfGFP (primers eGFPa2F and eGFPa2R), as well as the promoter region upstream of the *S. meliloti* Rm1021 *cspA2* (SMc01428) gene (genomic region spanning from position 2272810 to 2273098) using primers a2promF and a2promR. These amplicons were digested and ligated together, and the *cspA2p::eGFP* fusion product was cloned into pK19 *mob sacB* using digestion enzymes listed in Table S1. The *cspA2* promoter was chosen because it is highly active in free-living cells and in symbiosis (48). The *cspA2p::eGFP* construct showed no observable impact on symbiosis (Fig. 4) or zone specificity at 30 days postinoculation (Fig. 5J) and no free-living or symbiotic growth defects in mutants lacking the *cspA2* gene (data not shown). As with previous pK19 constructs, this plasmid was transformed into *E. coli* S17-1 and recombined into *S. meliloti* Rm1021 via biparental mating. The position of each eGFP-tagged construct after homologous recombination into the *S. meliloti* chromosome was confirmed using PCR with a forward primer located upstream of the native gene (e.g., 600 bp upstream of SMc01903) and an eGFP reverse primer (GFPintegR [Table S1]).

Construction of Rm1021 deletion mutants. To investigate the extent to which HslUV and ClpP1 are involved in symbiosis, we constructed deletions of *hslU*, *hslV*, and *clpP1* and a double deletion of *hslUV* using the double homologous recombination method (46). Briefly, ~500 bp upstream and ~500 bp downstream of the target gene were amplified, digested, and ligated together. This ligation product was then cloned into pK19 *mob sacB* (49), transformed into *E. coli* S17-1, and biparentally mated into *S. meliloti* Rm1021. $MMNH_4$ containing 200 μg/ml neomycin was used to select for *S. meliloti* containing the pK19-derived plasmid integrated into the chromosome as a result of homologous recombination between the *S. meliloti* sequences on the plasmid and similar sequences in the chromosome. The Neo^r *S. meliloti* strains isolated in this way were then grown on LB agar plus 1% sucrose to select for loss of the *sacB* gene carried on pK19 via a second homologous recombination. Colonies were then screened for recombinants that lacked the corresponding target gene (e.g., *hslU*, *hslV*, or *clpP1*) using PCR to confirm the absence of the target gene in *S. meliloti* with upstream and downstream primers listed in Table S1.

Free-living growth curves and EPS visualization. Wild-type *S. meliloti* Rm1021 and the Δ*hslU*, Δ*hslV*, Δ*hslUV*, and Δ*clpP1* deletion mutants were grown overnight as biological triplicates in 100 ml of $MMNH_4$ to produce large cultures synchronized to the same growth phase. The cultures were then spun down, washed with and resuspended in 0.85% NaCl, normalized by A_{600} to a value of 1.0, and used to inoculate 5-ml subcultures at a 1:100 ratio in the case of cultures grown at both 30°C and 37°C and at a 1:20 ratio for cultures grown in LB at 30°C supplemented with kanamycin at 50 μg/ml. Cultures were allowed to continue shaking at 250 rpm at either 30°C, 45°C, or 30°C with 50 μg/ml kanamycin. To visualize the exopolysaccharide (EPS) phenotypes of the deletion mutants compared to the wild type, spot tests were performed by a procedure similar to that described previously (50). Briefly, Δ*hslU*, Δ*hslV*, Δ*hslUV*, Δ*clpP1*, and wild-type Rm1021 were each grown in biological triplicate 5-ml $MMNH_4$ cultures to an A_{600} of 0.5. Each culture was then spun down, washed twice with and resuspended in 0.85% NaCl, and normalized by A_{600} to a value of 0.5. These cultures were then serially 5-fold diluted in a 96-well plate and spotted using a 96-prong inoculating manifold onto both LB and $MMNH_4$ plates, both with and without 0.02% calcofluor white (Fluorescent Brightener 28; Sigma no. F3543) (50). These plates were then incubated at 30°C for an additional 48 h and visualized under UV light. The intensity of each colony was analyzed using the Fiji image analysis package (51).

HslUV- and ClpXP-eGFP nodule visualization. Twenty-eight-day-old nodules were excised from roots and bisected longitudinally using a scalpel. Each half was then placed into a depression well slide submerged in Prolong Gold with 4′,6-diamidino-2-phenylindole (DAPI) (Thermo Fisher Scientific no. P36935). Each sample was visualized using a Leica SP8-X fluorescence microscope at magnifications of ×20 and ×200. Images were analyzed using Leica Analysis Suite version 2.0 and the Fiji image analysis package (51).

Co-IP. For free-living coimmunoprecipitations (co-IPs), *S. meliloti* Rm1021 strains containing endogenously eGFP-tagged *hslU*, *hslV*, *clpX*, and *clpP1*, as well as *cspA2p::eGFP*, were grown on $MMNH_4$ at 30°C with shaking until they reached an A_{600} of 0.7. The cells were then spun at 6,000 × *g*, washed once, and resuspended in ice-cold lysis buffer (20 mM Tris [pH 7.5], 150 mM NaCl, 1 mM dithiothreitol [DTT], 0.1% Tween 20). Cells were sonicated on ice 4 times for 10 s at amplitude 10 using a QSonica model Q700 sonifier. For nodule co-IPs, approximately 50 nodules were collected from *M. sativa* plants at 28 days

postinoculation with each eGFP-tagged strain. These nodules were pulverized in a bead mill (TissueLyser II Retsch MM400; Qiagen) and resuspended in ice-cold lysis buffer (as described above). For both free-living and nodule co-IPs, the cell lysate was spun at 45,000 × *g* for 15 min at 4°C. The supernatant was then incubated with anti-GFP nano-antibody-conjugated agarose beads (Allele Biotechnology no. ABP-nAb-GFPA050) for 15 min and then split into two different tubes. The first tube was washed twice with 10 resin bed volumes of wash buffer (lysis buffer without Tween 20). The second tube was washed twice with 100 resin bed volumes of wash buffer. The two wash methods were used to investigate both weak and strong protein-protein interactions. Samples were then eluted with twice the resin bed volume of elution buffer (200 mM glycine, pH 2.5), which was immediately neutralized using 1 M Tris (pH 9.5) to generate a final concentration of 100 mM Tris and a pH of ~8.0.

Western blot visualization of proteins. Protein samples were first separated using NuPAGE 10% Bis-Tris protein gels (Thermo Fisher Scientific, NP0301BOX) containing MES (morpholineethanesulfonic acid) buffer. Protein was then transferred by electrophoresis for 1 h at 30 V (DC) (~170 mA) in transfer buffer (25 mM Tris base, 200 mM glycine, 20% methanol) onto Immobilon polyvinylidene difluoride (PVDF) membranes (EMD Millipore, IPVH15150). Membranes were then blocked for 2 h using TBST buffer (25 mM Tris base, 150 mM NaCl, 0.1% Tween 20, pH 7.2) containing 5% (wt/vol) powdered milk. Blocked membranes were then probed overnight with chromatin immunoprecipitation (ChIP) grade rabbit anti-GFP primary antibodies (Abcam, ab290) at a dilution of 1:5,000 in TBST containing 2.5% (wt/vol) powdered milk. After three 15-min washes with TBST, the membranes were probed for 1 h with horseradish peroxidase-conjugated goat anti-rabbit secondary antibodies (Abcam, ab97080). The membranes were washed in TBST and visualized using SuperSignal West Pico Plus chemiluminescent substrate (Thermo Fisher Scientific, catalog no. 34580) according to the manufacturer's protocol.

Stress tests, cDNA synthesis, and qPCR. Biological triplicates of *S. meliloti* Rm1021 were grown in 5 ml liquid $MMNH_4$ cultures at 30°C with shaking at 250 rpm until they reached an A_{600} of 0.5. One set of biological triplicates was allowed to continue growing under these conditions, while the other sets of biological triplicate cultures were subjected to different stresses, including heat shock (45°C), cold shock (4°C), elevated salt shock (from 85 mM NaCl to a final concentration of 300 mM), neomycin shock (200 μg/ml neomycin), and treatment with H_2O_2 (final H_2O_2 concentration of 1 mM). At 15 and 60 min poststress, each "stressed" culture, as well as the unstressed control, was rapidly cooled in an ice-water bath for 5 min to halt transcription, spun down, washed once in ice-cold phosphate-buffered saline (PBS) (pH 7.5), and sonicated on ice 4 times for 10 s. The lysed cells were then centrifuged at 15,000 × *g* for 10 min, and the resulting supernatant was added to TRIzol at a ratio of 1:10. Chloroform was then added to the TRIzol-lysate mixture at a ratio of 1:5 of the starting TRIzol volume (i.e., 200 μl chloroform to 1,000 μl TRIzol). This was shaken vigorously and spun at 12,000 × *g* for 15 min at 4°C. The aqueous top layer was isolated, and the RNA was precipitated using isopropanol at a ratio of 1:2 ml TRIzol reagent used for initial extraction. The RNA pellet was then washed with 75% ethanol, resuspended in RNase-free water, and quantified using a Nanodrop spectrophotometer. Conversion of RNA to cDNA was accomplished using the Superscript III first-strand synthesis system (Invitrogen, 18080-400) using the manufacturer's protocols and random hexamer primers. qPCR was conducted using Fast SYBR green master mix (Applied Biosystems no. 4385612) with 23S rRNA as an endogenous control (SMc02939). All relevant primers used for qPCR are listed in Table S1.

LC-MS/MS parameters. Protein eluted from coimmunoprecipitation experiments was quantified with the Qubit protein assay kit (no. Q33211) using a Qubit 2.0 fluorimeter. Each sample was then normalized to contain the same amount of protein, subjected to trypsin digestion with Pierce MS grade trypsin protease (90057) using the manufacturer's protocols, and subsequently dried under vacuum. The dried samples were dissolved in 4% acetonitrile containing 0.1% formic acid (FA). The tryptic peptide mixtures were separated on a Thermo Fisher Scientific PepMap 100 C_{18} column (2 μm; 50 μm by 25 cm) using an Easy-nLC 1000 ultra-high-pressure liquid chromatograph (LC) and then analyzed on a Thermo Fisher Scientific Orbitrap Fusion Tribrid mass spectrometer. The peptides were separated over a 100-min gradient eluted at 300 nl/min with 0.1% FA in water (solvent A) and 0.1% FA in acetonitrile (solvent B) (3% to 35% B in 100 min, followed by 35% to 93% B over 5 min and holding the 93% B for 10 min). MS1 data were acquired on the Orbitrap with a full-scan method using the following parameters: scan range, *m/z* 400 to 1500; Orbitrap resolution, 120,000; AGC target, 2.0×10^5; and maximum injection time, 100 ms. The precursors were selected using monoisotopic peak determination with a charge state of 2 to 7 and filtered by a dynamic exclusion window of 60 s with an intensity threshold of 4.0×10^3. MS2 was performed on the top 20 data-dependent scans that had been detected in the ion trap and collected using the following parameters: quadrupole isolation mode, isolation window of 1.6 *m/z*, HCD collision energy of 35%, AGC of 1.0×10^4, and maximum injection time of 35 ms.

Using Thermo Scientific Proteome Discoverer software (version 2.1), the obtained LC-MS/MS spectra were searched for matches in a FASTA file of protein sequences generated from UniProtKB/Swiss-Prot databases of *S. meliloti* Rm1021 for free-living samples or in a FASTA file that combined *S. meliloti* Rm1021 and *Medicago truncatula* protein predictions in the case of nodule samples (52). The searching parameters included a maximum missed cleavage of 2, a precursor mass tolerance of 10 ppm, and a fragmentation mass tolerance of 0.6 Da. The static peptide modification was carbamidomethylation (+57.021 Da) on cysteine. The dynamic modifications included acetylation (+42.011 Da) on N termini and lysine, oxidation (+15.995 Da) on methionine and lysine, and phosphorylation (+79.966 Da) on serine, threonine, and tyrosine. The target false-discovery rates (FDR) for decoy database search were 1% for strict and 5% for relaxed.

SUPPLEMENTAL MATERIAL

Supplemental material for this article may be found at https://doi.org/10.1128/JB.00498-18.

SUPPLEMENTAL FILE 1, XLSX file, 0.01 MB.
SUPPLEMENTAL FILE 2, XLSX file, 1.5 MB.
SUPPLEMENTAL FILE 3, XLSX file, 1.3 MB.
SUPPLEMENTAL FILE 4, XLSX file, 0.05 MB.
SUPPLEMENTAL FILE 5, PDF file, 2.2 MB.

ACKNOWLEDGMENTS

This work was supported in part by a Loyal Davis Endowed Fellowship to A.J.O. from the Institute of Biological Chemistry at Washington State University, as well as predoctoral fellowship DGE-1347973 to A.J.O. from the U.S. National Science Foundation. Further support was provided by a Protein Biotechnology predoctoral traineeship (T32GM008336) to A.J.O. from the U.S. National Institutes of Health, National Institute of General Medical Sciences. J.M.M. was supported by an REU associated with grant 1645590 from the U.S. National Science Foundation. Research support was obtained from grant DE-FG03-96ER20225 to M.L.K. from the U.S. Department of Energy-Basic Energy Sciences-Physical Biosciences Program and from USDA-NIFA through the College of Agricultural, Human and Natural Resource Sciences at Washington State University.

REFERENCES

1. Soupène E, Foussard M, Boistard P, Truchet G, Batut J. 1995. Oxygen as a key developmental regulator of Rhizobium meliloti N2-fixation gene expression within the alfalfa root nodule. Proc Natl Acad Sci U S A 92:3759–3763. https://doi.org/10.1073/pnas.92.9.3759.
2. Tiricz H, Szűcs A, Farkas A, Pap B, Lima RM, Maróti G, Kondorosi É, Kereszt A. 2013. Antimicrobial nodule-specific cysteine-rich peptides induce membrane depolarization-associated changes in the transcriptome of Sinorhizobium meliloti. Appl Environ Microbiol 79:6737–6746. https://doi.org/10.1128/AEM.01791-13.
3. Mellor RB. 1989. Bacteroids in the Rhizobium-legume symbiosis inhabit a plant internal lytic compartment: implications for other microbial endosymbioses. J Exp Bot 40:831–839. https://doi.org/10.1093/jxb/40.8.831.
4. Pierre O, Engler G, Hopkins J, Brau F, Boncompagni E, Herouart D. 2013. Peribacteroid space acidification: a marker of mature bacteroid functioning in Medicago truncatula nodules. Plant Cell Environ 36:2059–2070. https://doi.org/10.1111/pce.12116.
5. Vedam V, Kannenberg EL, Haynes JG, Sherrier DJ, Datta A, Carlson RW. 2003. A Rhizobium leguminosarum AcpXL mutant produces lipopolysaccharide lacking 27-hydroxyoctacosanoic acid. J Bacteriol 185:1841–1850. https://doi.org/10.1128/JB.185.6.1841-1850.2003.
6. Santos R, Hérouart D, Sigaud S, Touati D, Puppo A. 2001. Oxidative burst in alfalfa-Sinorhizobium meliloti symbiotic interaction. Mol Plant Microbe Interact 14:86–89. https://doi.org/10.1094/MPMI.2001.14.1.86.
7. Sallet E, Roux B, Sauviac L, Jardinaud M-F, Carrère S, Faraut T, de Carvalho-Niebel F, Gouzy J, Gamas P, Capela D, Bruand C, Schiex T. 2013. Next-generation annotation of prokaryotic genomes with EuGene-P: application to Sinorhizobium meliloti 2011. DNA Res 20:339–354. https://doi.org/10.1093/dnares/dst014.
8. Roux B, Rodde N, Jardinaud M-F, Timmers T, Sauviac L, Cottret L, Carrère S, Sallet E, Courcelle E, Moreau S, Debellé F, Capela D, de Carvalho-Niebel F, Gouzy J, Bruand C, Gamas P. others. 2014. An integrated analysis of plant and bacterial gene expression in symbiotic root nodules using laser-capture microdissection coupled to RNA sequencing. Plant J 77:817–837. https://doi.org/10.1111/tpj.12442.
9. Ogden AJ, Gargouri M, Park J, Gang DR, Kahn ML. 2017. Integrated analysis of zone-specific protein and metabolite profiles within nitrogen-fixing Medicago truncatula-Sinorhizobium medicae nodules. PLoS One 12:e0180894. https://doi.org/10.1371/journal.pone.0180894.
10. Sauer RT, Baker TA. 2011. AAA+ Proteases: ATP-fueled machines of protein destruction. Annu Rev Biochem 80:587–612. https://doi.org/10.1146/annurev-biochem-060408-172623.
11. Neher SB, Villén J, Oakes EC, Bakalarski CE, Sauer RT, Gygi SP, Baker TA. 2006. Proteomic profiling of ClpXP substrates after DNA damage reveals extensive instability within SOS regulon. Mol Cell 22:193–204. https://doi.org/10.1016/j.molcel.2006.03.007.
12. Kobayashi H, De Nisco NJ, Chien P, Simmons LA, Walker GC. 2009. Sinorhizobium meliloti CpdR1 is critical for co-ordinating cell cycle progression and the symbiotic chronic infection. Mol Microbiol 73:586–600. https://doi.org/10.1111/j.1365-2958.2009.06794.x.
13. Schweder T, Lee KH, Lomovskaya O, Matin A. 1996. Regulation of Escherichia coli starvation sigma factor (sigma s) by ClpXP protease. J Bacteriol 178:470–476. https://doi.org/10.1128/jb.178.2.470-476.1996.
14. Xu X, Niu Y, Liang K, Wang J, Li X, Yang Y. 2015. Heat shock transcription factor δ32 is targeted for degradation via an ubiquitin-like protein ThiS in Escherichia coli. Biochem Biophys Res Commun 459:240–245. https://doi.org/10.1016/j.bbrc.2015.02.087.
15. Chang C-Y, Hu H-T, Tsai C-H, Wu W-F. 2016. The degradation of RcsA by ClpYQ(HslUV) protease in Escherichia coli. Microbiol Res 184:42–50. https://doi.org/10.1016/j.micres.2016.01.001.
16. Lau-Wong IC, Locke T, Ellison MJ, Raivio TL, Frost LS. 2008. Activation of the Cpx regulon destabilizes the F plasmid transfer activator, TraJ, via the HslVU protease in Escherichia coli. Mol Microbiol 67:516–527. https://doi.org/10.1111/j.1365-2958.2007.06055.x.
17. Liang W, Deutscher MP. 2012. Transfer-messenger RNA-SmpB protein regulates ribonuclease R turnover by promoting binding of HslUV and Lon proteases. J Biol Chem 287:33472–33479. https://doi.org/10.1074/jbc.M112.375287.
18. Hellweg C, Pühler A, Weidner S. 2009. The time course of the transcriptomic response of Sinorhizobium meliloti 1021 following a shift to acidic pH. BMC Microbiol 9:37. https://doi.org/10.1186/1471-2180-9-37.
19. Hamilton TL, Ludwig M, Dixon R, Boyd ES, Santos PCD, Setubal JC, Bryant DA, Dean DR, Peters JW. 2011. Transcriptional profiling of nitrogen fixation in Azotobacter vinelandii. J Bacteriol 193:4477–4486. https://doi.org/10.1128/JB.05099-11.
20. Schlüter J-P, Reinkensmeier J, Barnett MJ, Lang C, Krol E, Giegerich R, Long SR, Becker A. 2013. Global mapping of transcription start sites and promoter motifs in the symbiotic α-proteobacterium Sinorhizobium meliloti1021. BMC Genomics 14:156. https://doi.org/10.1186/1471-2164-14-156.
21. Sauviac L, Philippe H, Phok K, Bruand C. 2007. An extracytoplasmic function sigma factor acts as a general stress response regulator in Sinorhizobium meliloti. J Bacteriol 189:4204–4216. https://doi.org/10.1128/JB.00175-07.

22. Leigh JA, Signer ER, Walker GC. 1985. Exopolysaccharide-deficient mutants of Rhizobium meliloti that form ineffective nodules. Proc Natl Acad Sci U S A 82:6231–6235. https://doi.org/10.1073/pnas.82.18.6231.
23. Shimoda Y, Shinpo S, Kohara M, Nakamura Y, Tabata S, Sato S. 2008. A large scale analysis of protein-protein interactions in the nitrogen-fixing bacterium Mesorhizobium loti. DNA Res 15:13–23. https://doi.org/10.1093/dnares/dsm028.
24. Flynn JM, Neher SB, Kim Y-I, Sauer RT, Baker TA. 2003. Proteomic discovery of cellular substrates of the ClpXP protease reveals five classes of ClpX-recognition signals. Mol Cell 11:671–683. https://doi.org/10.1016/S1097-2765(03)00060-1.
25. Hu P, Janga SC, Babu M, Díaz-Mejía JJ, Butland G, Yang W, Pogoutse O, Guo X, Phanse S, Wong P, Chandran S, Christopoulos C, Nazarians-Armavil A, Nasseri NK, Musso G, Ali M, Nazemof N, Eroukova V, Golshani A, Paccanaro A, Greenblatt JF, Moreno-Hagelsieb G, Emili A. 2009. Global functional atlas of Escherichia coli encompassing previously uncharacterized proteins. PLoS Biol 7:e1000096. https://doi.org/10.1371/journal.pbio.1000096.
26. Butland G, Peregrín-Alvarez JM, Li J, Yang W, Yang X, Canadien V, Starostine A, Richards D, Beattie B, Krogan N, Davey M, Parkinson J, Greenblatt J, Emili A. 2005. Interaction network containing conserved and essential protein complexes in *Escherichia coli*. Nature 433:531–537. https://doi.org/10.1038/nature03239.
27. Arifuzzaman M, Maeda M, Itoh A, Nishikata K, Takita C, Saito R, Ara T, Nakahigashi K, Huang H-C, Hirai A, Tsuzuki K, Nakamura S, Altaf-Ul-Amin M, Oshima T, Baba T, Yamamoto N, Kawamura T, Ioka-Nakamichi T, Kitagawa M, Tomita M, Kanaya S, Wada C, Mori H. 2006. Large-scale identification of protein-protein interaction of Escherichia coli K-12. Genome Res 16:686–691. https://doi.org/10.1101/gr.4527806.
28. Rajagopala SV, Sikorski P, Kumar A, Mosca R, Vlasblom J, Arnold R, Franca-Koh J, Pakala SB, Phanse S, Ceol A, Häuser R, Siszler G, Wuchty S, Emili A, Babu M, Aloy P, Pieper R, Uetz P. 2014. The binary protein-protein interaction landscape of *Escherichia coli*. Nat Biotechnol 32:285–290. https://doi.org/10.1038/nbt.2831.
29. Szklarczyk D, Franceschini A, Wyder S, Forslund K, Heller D, Huerta-Cepas J, Simonovic M, Roth A, Santos A, Tsafou KP, Kuhn M, Bork P, Jensen LJ, von Mering C. 2015. STRING v10: protein-protein interaction networks, integrated over the tree of life. Nucleic Acids Res 43:D447–D452. https://doi.org/10.1093/nar/gku1003.
30. Huang DW, Sherman BT, Tan Q, Collins JR, Alvord WG, Roayaei J, Stephens R, Baseler MW, Lane HC, Lempicki RA. 2007. The DAVID gene functional classification tool: a novel biological module-centric algorithm to functionally analyze large gene lists. Genome Biol 8:R183. https://doi.org/10.1186/gb-2007-8-9-r183.
31. Nielsen H. 2017. Predicting secretory proteins with SignalP. Methods Mol Biol 1611:59–73. https://doi.org/10.1007/978-1-4939-7015-5_6.
32. Lehman AP, Long SR. 2018. OxyR-dependent transcription response of Sinorhizobium meliloti to oxidative stress. J Bacteriol 200:e00622-17. https://doi.org/10.1128/JB.00622-17.
33. Kotra LP, Haddad J, Mobashery S. 2000. Aminoglycosides: perspectives on mechanisms of action and resistance and strategies to counter resistance. Antimicrob Agents Chemother 44:3249–3256. https://doi.org/10.1128/AAC.44.12.3249-3256.2000.
34. Lin JT, Connelly MB, Amolo C, Otani S, Yaver DS. 2005. Global transcriptional response of Bacillus subtilis to treatment with subinhibitory concentrations of antibiotics that inhibit protein synthesis. Antimicrob Agents Chemother 49:1915–1926. https://doi.org/10.1128/AAC.49.5.1915-1926.2005.
35. Pechmann S, Willmund F, Frydman J. 2013. The ribosome as a hub for protein quality control. Mol Cell 49:411–421. https://doi.org/10.1016/j.molcel.2013.01.020.
36. Ferbitz L, Maier T, Patzelt H, Bukau B, Deuerling E, Ban N. 2004. Trigger factor in complex with the ribosome forms a molecular cradle for nascent proteins. Nature 431:590–596. https://doi.org/10.1038/nature02899.
37. Deuerling E, Schulze-Specking A, Tomoyasu T, Mogk A, Bukau B. 1999. Trigger factor and DnaK cooperate in folding of newly synthesized proteins. Nature 400:693–696. https://doi.org/10.1038/23301.
38. Teter SA, Houry WA, Ang D, Tradler T, Rockabrand D, Fischer G, Blum P, Georgopoulos C, Hartl FU. 1999. Polypeptide flux through bacterial Hsp70: DnaK cooperates with trigger factor in chaperoning nascent chains. Cell 97:755–765. https://doi.org/10.1016/S0092-8674(00)80787-4.
39. Ying B-W, Taguchi H, Kondo M, Ueda T. 2005. Co-translational involvement of the chaperonin GroEL in the folding of newly translated polypeptides. J Biol Chem 280:12035–12040. https://doi.org/10.1074/jbc.M500364200.
40. Ying B-W, Taguchi H, Ueda T. 2006. Co-translational binding of GroEL to nascent polypeptides is followed by post-translational encapsulation by GroES to mediate protein folding. J Biol Chem 281:21813–21819. https://doi.org/10.1074/jbc.M603091200.
41. Wang S, Yang C-I, Shan S. 2017. SecA mediates cotranslational targeting and translocation of an inner membrane protein. J Cell Biol 216:3639–3653. https://doi.org/10.1083/jcb.201704036.
42. Randall LL, Topping TB, Hardy SJS, Pavlov MY, Freistroffer DV, Ehrenberg M. 1997. Binding of SecB to ribosome-bound polypeptides has the same characteristics as binding to full-length, denatured proteins. Proc Natl Acad Sci U S A 94:802–807. https://doi.org/10.1073/pnas.94.3.802.
43. Green MR, Sambrook J. 2012. Molecular cloning: a laboratory manual. Cold Spring Harbor Laboratory Press, Cold Spring Harbor, NY.
44. Barker DG, Pfaff T, Moreau D, Groves E, Ruffel S, Lepetit M, Whitehand S, Maillet F, Nair RM, Journet E-P. 2006. Growing M. truncatula: choice of substrates and growth conditions. *In* The Medicago truncatula handbook. The Samuel Roberts Noble Foundation, Ardmore, OK. http://www.noble.org/medicago-handbook/.
45. Pédelacq J-D, Cabantous S, Tran T, Terwilliger TC, Waldo GS. 2006. Engineering and characterization of a superfolder green fluorescent protein. Nat Biotechnol 24:79–88. https://doi.org/10.1038/nbt1172.
46. Yurgel SN, Kahn ML. 2005. Sinorhizobium meliloti dctA mutants with partial ability to transport dicarboxylic acids. J Bacteriol 187:1161–1172. https://doi.org/10.1128/JB.187.3.1161-1172.2005.
47. Simon R, Priefer U, Pühler A. 1983. Vector plasmids for in vivo and in vitro manipulations of gram-negative bacteria, p 98–106. *In* Pühler A (ed), Molecular genetics of the bacterial-plant interaction: the Rhizobium meliloti-Medicago sativa system. Springer, Berlin, Germany.
48. Price J. 2017. Control of RNA structure by CspA proteins in rhizobia. Ph.D. thesis. Washington State University, Pullman, WA.
49. Schäfer A, Tauch A, Jäger W, Kalinowski J, Thierbach G, Pühler A. 1994. Small mobilizable multi-purpose cloning vectors derived from the Escherichia coli plasmids pK18 and pK19: selection of defined deletions in the chromosome of Corynebacterium glutamicum. Gene 145:69–73. https://doi.org/10.1016/0378-1119(94)90324-7.
50. Gibson KE, Campbell GR, Lloret J, Walker GC. 2006. CbrA is a stationary-phase regulator of cell surface physiology and legume symbiosis in Sinorhizobium meliloti. J Bacteriol 188:4508–4521. https://doi.org/10.1128/JB.01923-05.
51. Schindelin J, Arganda-Carreras I, Frise E, Kaynig V, Longair M, Pietzsch T, Preibisch S, Rueden C, Saalfeld S, Schmid B, Tinevez J-Y, White DJ, Hartenstein V, Eliceiri K, Tomancak P, Cardona A. 2012. Fiji: an open-source platform for biological-image analysis. Nat Methods 9:676–682. https://doi.org/10.1038/nmeth.2019.
52. UniProt Consortium. 2015. UniProt: a hub for protein information. Nucleic Acids Res 43:D204–D212. https://doi.org/10.1093/nar/gku989.